Research Article Open Access

Fa-Jun Zhao*, Yun-Long Wang, Jun Song, Hai-Cheng Ma, Hao-Liang Liu

Performance and thermal decomposition analysis of foaming agent NPL-10 for use in heavy oil recovery by steam injection

https://doi.org/10.1515/chem-2018-0002
received August 18, 2017; accepted October 27, 2017.

Abstract: Foaming agents, despite holding potential in steam injection technology for heavy oil recovery, are still poorly investigated. In this work, we analyzed the performance of the foaming agent NPL-10 in terms of foam height and half-life under various conditions of temperature, pH, salinity, and oil content by orthogonal experiments. The best conditions of use for NPL-10 among those tested are T=220°C, pH 7, salinity 10000 mg·L^{-1}, and oil content 10 g·L^{-1}. Thermal decomposition of NPL-10 was also studied by thermogravimetric and differential thermal analyses. NPL-10 decomposes above 220°C, and decomposition is a two-step process. The kinetic triplet (activation energy, kinetic function and pre-exponential factor) and the corresponding rate law were calculated for each step. Steps 1 and 2 follow kinetics of different order (n = 2 and ½, respectively). These findings provide some criteria for the selection of foaming agents for oil recovery by steam injection.

Keywords: thermal recovery, foam flooding, foaming agent, foamability, thermal decomposition.

1 Introduction

The extraction of heavy crude oil from reservoirs is usually carried out by steam injection. There are several forms of the technology, with the major ones being steam stimulation, steam flooding, and steam-assisted gravity drainage [1,2]. The main challenge in the use of steam for heavy oil recovery is steam channeling, *i.e.*, the ability to make steam flow in a single direction (from the injector to the extractor) in such a way as to maximize the extraction yield. Another problem posed by steam injection is that steam can seriously damage the underground well structure. This phenomenon can endanger the lives of workers while resulting into thermal dispersion and poor mining effect [3-5]. Heavy oil reservoirs in China are quite heterogeneous in terms of layer permeability, thus requiring highly different conditions for optimal steam channeling [4,5]. Foams can improve steam channeling and enhance oil recovery by reducing the surface tension and viscosity of fluids [6-9]. However, the use of foaming agents in heavy oil recovery is still limited due to the small number of studies on the behavior of such agents at high temperature and salinity, which prevents the selection of the most appropriate agent.

In this work, we analyzed the performance of a high temperature foaming agent (NPL-10) in terms of foam height and half-life in order to establish the optimal conditions of its use. The thermal decomposition process of NPL-10 was analyzed by thermogravimetric and differential thermal analyses, and the kinetics of non-isothermal decomposition was studied to quantify the effect of temperature on decomposition rate.

2 Experimental

2.1 Chemicals

Test solutions for orthogonal experiments were prepared using deionized water. Three solutions with different total concentrations (5000, 10000 and 15000 mg·L^{-1}) were used. Solutions had the following composition: 5000 mg·L^{-1} solution: $NaHCO_3$ 3000 mg·L^{-1}, NaCl 700 mg·L^{-1}; 10000 mg·L^{-1} solution: $NaHCO_3$ 6000 mg·L^{-1}, NaCl 1400 mg·L^{-1};

***Corresponding author: Fa-Jun Zhao:** Key Laboratory of Oil Recovery Enhance of Ministry of Education, Northeast Petroleum University, Daqing City, Heilongjiang province, China, 163318, E-mail: fajzhao@126.com
Yun-Long Wang, Jun Song: College of Chemistry and Chemical Engineering, Northeast Petroleum University, Daqing 163318, Heilongjiang, China
Hai-Cheng Ma, Hao-Liang Liu: College of Chemistry and Chemical Engineering, Northeast Petroleum University, Daqing 163318, Heilongjiang, China

Table 1: Orthogonal experimental data for foam height and half-life.

factors / entry	A T (°C)	B pH	C salinity (mg·L^{-1})	D oil density (g·L^{-1})	height/half-life (mm/min)
1	220	5	5000	0	255/13.5
2	220	7	10000	5	240/11.67
3	220	9	15000	10	230/10
4	260	5	10000	10	200/10.2
5	260	7	15000	0	220/11.5
6	260	9	5000	5	213/9
7	300	5	15000	5	11/1.01
8	300	7	5000	10	8/0.9
9	300	9	10000	0	9/0.93
K1	725/35.17	466/24.17	476/23.4	484/25.93	
K2	633/30.7	468/24.07	449/22.8	464/21.68	
K3	28/2.84	452/19.39	461/22.8	438/21.1	
k_1	241.67/11.72	155.33/8.23	158.67/7.8	161.33/8.64	
k_2	211/10.23	156/8.02	149.67/7.6	154.67/7.23	
k_3	9.33/0.95	150.67/6.64	153.67/7.5	146/7.03	
Range R	232.33/10.78	5.34/1059	9/0.3	15.33/1.61	
Secondary sequence	A>B>C>D / A>D>B>C				
Optimized combination	$A_1B_2C_2D_3$				

K1, K2, K3 are the sum of the level 1, 2, and 3 data on the corresponding factors, respectively.
k1, k2, k3 are the comprehensive average of 1, 2, and 3 level data, respectively.

15000 mg·L^{-1} solution: $NaHCO_3$ 9000 mg·L^{-1}, NaCl 2100 mg·L^{-1}. Concentrations of other ions were simulated by a water preparation and salinity calculation software. Heavy oil was collected from Du-66 block area of Liaohe Oilfield and dehydrated before use. Foaming agent NPL-10 (long-chain alpha olefin sulfonate) was prepared according to literature [10,11], and had purity >97%.

2.2 Methods

Reactions were performed in a high temperature, high pressure reaction kettle WYF-1 supplied by Haian Jiangsu oil factory. Foamability and foam stability were determined by a 2151 Roche foam instrument (standard form) using a customized GB/T 7462-94 Ross-Miles method. Thermogravimetric and differential thermal analyses were carried out by a thermal analyzer DuPont 2100 (Perkin Elmer, USA) under nitrogen.

Ethical approval: This research is not related to human or animal use.

3 Results and discussion

3.1 Performance analysis of NPL-10

We studied the effect of four factors (temperature, salinity, pH, and oil content) on the foam height and half-life of NPL-10 by orthogonal experiments [12-14]. The height and half-life of NPL-10 foam were measured under various combinations of *T* (220, 260, and 300°C), pH (5, 7, and 9), salinity (5000, 10000, and 15000 mg·L^{-1}) and oil content (0, 5, and 10 g·L^{-1}; Table 1). The sensitivity of foam height and half-life to each factor was examined by a trend chart (Figure 1). Results showed that foam height and half-life depend on temperature (A), pH (B), salinity (C) and oil content (D) to a different extent (Figure 1). At 220°C, the order of factors observed for foam height is A>B>C>D; in other words, foam height mainly depends on temperature. Foam height decreases sharply on increasing temperature, and the most marked decrease is observed when temperature rises from 260°C to 300°C. Conversely, an

increase in the other factors (pH, salinity and oil content) has almost no effect on foam height.

The order of factors observed for foam half-life at 220°C is A>D>C>B. The most important factor for foam half-life is still temperature, but the second one is the oil content, not pH. Analogously to foam height, foam half-life decreases significantly on increasing temperature but is not significantly influenced by other factors.

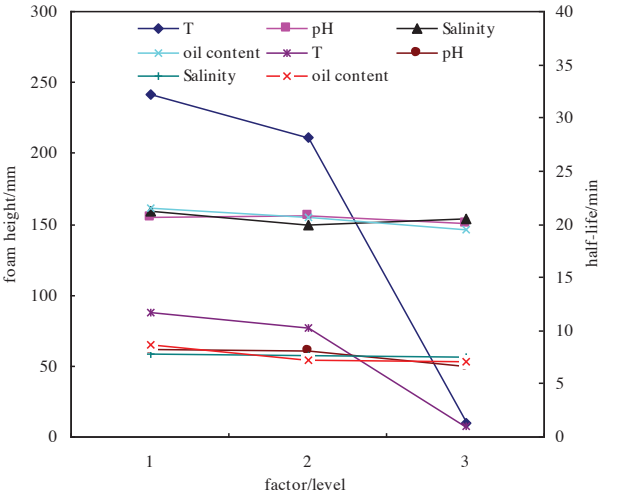

Figure 1: NPL-10 trend chart of factors at three different levels. Level 1 = 220°C, level 2 = 260°C; level 3 = 300°C. Top lines (dark blue, light blue, black and pink): effect on foam height. Bottom lines (violet, red, brown, green): effect on foam half-life.

3.2 Thermal decomposition of NPL-10

After determining the best conditions of use for NPL-10, we studied its thermal decomposition process by non-isothermal thermogravimetric analysis (TGA) and differential thermal analysis (DTA) [15-18].

3.2.1 Non-isothermal thermogravimetric analysis (TGA) and differential thermal analysis (DTA)

Non-isothermal thermogravimetric analysis (TGA) and differential thermal analysis (DTA) were carried out at three different heating rates (5, 15, and 20 K·min^{-1}). TGA indicated that, regardless of heating rate, NPL-10 starts decomposing at about 250°C, and decomposition is complete at about 500°C (Figure 2). DTA highlighted that thermal decomposition is a two-step process: the first decomposition step occurs at 200–300°C, with a mass loss of 4–26%; the second step occurs at 300–400°C, with 15–59% mass loss (Figure 3). Both steps are endothermic. Furthermore, both the rate of mass loss and the peak temperature of thermal decomposition gradually increase on increasing the heating rate.

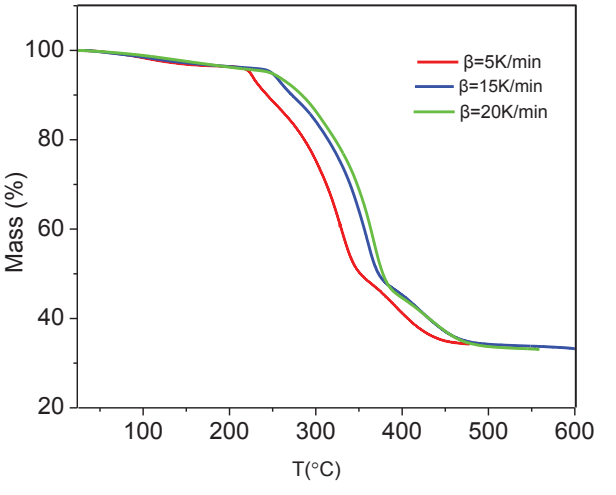

Figure 2: Thermogravimetric analysis (TGA) curve of NPL-1.

3.2.2 Kinetics of thermal decomposition reaction

The thermal decomposition rate can be expressed by Eq. (1) as a function of two independent variables: the transformation rate α and temperature T [19]:

$$\left(\frac{d\alpha}{dt}\right)_T = k(T)\, f(\alpha) \tag{1}$$

where T (K) is the absolute temperature of sample, α (%) is the decomposition rate, and k is the rate constant for the decomposition reaction. The heating rate β is constant in GTA and DTA, and is expressed by Eq. (2):

$$\beta = dT/dt \tag{2}$$

The rate constant k depends on temperature T according to the Arrhenius equation [20]:

$$k(T) = A\exp\left(-\frac{E_a}{RT}\right) \tag{3}$$

where A is the pre-exponential factor (s^{-1}), E_a is the activation energy (J·mol^{-1}), and R is the gas constant (8.314 J·mol^{-1}·K^{-1}).

Combining Eqs. (1), (2) and (3) provides Eq. (4), which is the rate law for the decomposition reaction:

$$\frac{d\alpha}{dT} = \frac{1}{\beta} A\exp\left(-\frac{E_a}{RT}\right) f(\alpha) \tag{4}$$

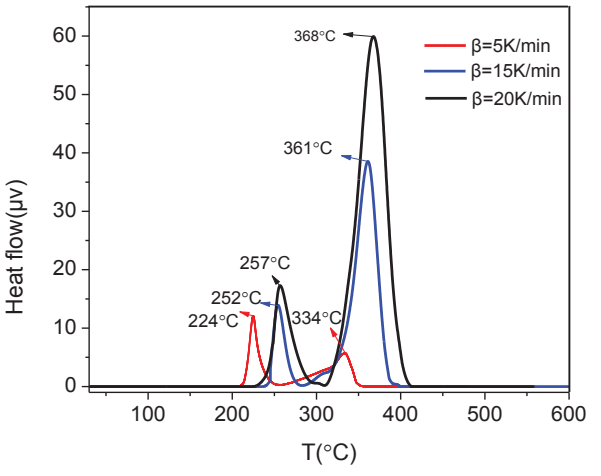

Figure 3: Differential thermal analysis (DTA) curve of NPL-10.

We calculated the kinetic triplet (the activation energy E_a, the pre-exponential factor A, and the mechanism function $g(\alpha)$) for both steps of NPL-10 decomposition process.

The activation energy E_a was obtained by Eq. (5) using KAS iterative method:

$$\ln\frac{\beta}{h(x)T^2}=\ln\left[\frac{AE_a}{g(\alpha)R}\right]-\frac{E_a}{RT} \tag{5}$$

where:

$$h(x)=\frac{x^4+18x^3+88x^2+96x}{x^4+20x^3+120x^2+240x+120} \tag{6}$$

and

$$x=\frac{E_a}{RT} \tag{7}$$

KAS iterative method is divided into three steps: ① Assume $h(x)$=1 to estimate the initial activation energy E_1 for given β and $g(\alpha)$ values by Eq. (5). ② Bring E_1 and the corresponding T into Eq. (7), then use the calculated x value to derive $h(x)$ by Eq. (6); enter x and $h(x)$ values into Eq. (5), and use the linear regression of $\ln[\beta/h(x)T^2]$ *vs* $1/T$ to calculate the line slope ($-E_2/R$) and hence E_2. ③ Repeat step ② by replacing E_1 by E_2. When $|E_i-E_{i-1}|<0.01$ kJ·mol^{-1}, E_i can be considered a real value.

The activation energy E_a was calculated for α = 0.2–0.8 at 0.05-unit intervals (Table 2). A plot of the activation energy E_a as a function of α for steps 1 and 2 (Figure 4) shows two curves of different shape, indicating that decomposition follows a different mechanism in steps 1 and 2. The non-linearity of curves suggests a complex mechanism for both steps.

To determine the most probable kinetic function $g(\alpha)$ for the thermal decomposition of NPL-10, we performed the linear regression analysis of 41 kinetic functions (Table 3) [18]. Eq. (5) was modified into Eq. (6):

Table 2: Activation energies calculated by KAS iterative method.

	E_a (kJ·mol^{-1})	
α (%)	step 1	step 2
0.2	72.56	68.41
0.25	68.94	69.79
0.3	66.02	71.41
0.35	63.78	72.87
0.4	62.07	74.44
0.45	60.95	76.16
0.5	59.95	78.00
0.55	59.21	79.28
0.6	59.05	80.37
0.65	58.78	80.34
0.7	58.86	78.00
0.75	59.16	71.79
0.8	59.40	76.24
average value	62.21	75.16

$$\ln g(\alpha)=\left[\ln\frac{AE}{R}+\ln\frac{e^{-x}}{x}+\ln p(x)\right]-\ln\beta \tag{6}$$

where

$$p(x)=\frac{e^{-x}}{x^2}h(x)\cdot$$

Linear regression analysis did not provide a straight line for four functions, namely 21 (dependent on pressure in addition to temperature), 25 (law of Mampel Power), 39 and 40 (both functions of index law). The kinetic functions with the slope closest to –1 and best R^2 values were $g(\alpha)=1-(1-\alpha)^2$ (Table 3, entry 33) for step 1 and $g(\alpha)=\alpha^{1/2}$ for step 2 of thermal decomposition (Table 3, entry 31). These results indicate that the two steps of thermal decomposition follow a different order of reaction (n=2 for step 1 and n=1/2 for step 2).

Pre-exponential factors A were calculated by entering E_a values (Table 2) and $g(\alpha)$ values (Table 3) into Eq. (5). The pre-exponential factor of step 1 is $A_1=3.86\cdot10^{11}$s^{-1}, the pre-exponential factor of step 2 is $A_2=5.60\cdot10^{13}$ s^{-1}. Calculation of E_a, $g(\alpha)$, and A allowed to derive the rate law of the decomposition process. The rate law for the first step of thermal decomposition is:

$$\frac{d\alpha}{dT}=\frac{3.86\cdot10^{11}}{\beta}\exp\left(-\frac{62.21\cdot10^3}{RT}\right)\cdot[1-(1-\alpha)^2];$$

the rate law for the second step is:

$$\frac{d\alpha}{dT}=\frac{5.60\cdot10^{13}}{\beta}\exp\left(-\frac{75.16\cdot10^3}{RT}\right)\cdot\alpha^{\frac{1}{2}}.$$

Table 3: Linear regression analysis of 41 kinetic functions for steps 1 and 2.

entry		step 1		step 2	
	g(α)	slope	R^2	slope	R^2
1	α^2	−3.0968	0.9339	−1.8111	0.8884
2	$\alpha+(1-\alpha)\ln(1-\alpha)$	−3.507	0.9522	−2.1661	0.918
3	$[1-(1-\alpha)^{1/2}]^{1/2}$	−0.4148	0.9984	−2.1661	0.918
4	$[1-(1-\alpha)^{1/2}]^2$	−0.4148	0.9984	−0.3096	0.9576
5	$[1-(1-\alpha)^{1/3}]^{1/2}$	−0.2479	0.9997	−0.1897	0.9669
6	$[1-(1-\alpha)^{1/3}]^2$	−0.4959	0.9997	−0.3794	0.9669
7	$1-2/3\alpha-(1-\alpha)^{2/3}$	0.4612	0.9765	0.4244	0.9981
8	$[(1+\alpha)^{1/3}-1]^2$	0.8862	0.9969	0.7346	0.9927
9	$[(1-\alpha)^{1/3}-1]^2$	−3.6837	0.9395	−3.9547	0.8843
10	$[-\ln(1-\alpha)]^{-1/4}$	−2.4013	0.9836	−1.6665	0.9699
11	$[-\ln(1-\alpha)]^{-1/3}$	−2.4013	0.9836	−1.6665	0.9699
12	$[-\ln(1-\alpha)]^{-2/3}$	−4.8026	0.9836	−3.3331	0.9699
13	$[-\ln(1-\alpha)]^{1/2}$	−2.4013	0.9836	−1.6665	0.9699
14	$[-\ln(1-\alpha)]^{2/3}$	−4.8026	0.9836	−3.3331	0.9699
15	$[-\ln(1-\alpha)]^{3/4}$	−7.2039	0.9836	−4.9996	0.9698
16	$-\ln(1-\alpha)$	−2.4013	0.9836	−1.6665	0.9699
17	$[-\ln(1-\alpha)]^{3/2}$	−7.2039	0.9836	−4.9996	0.9699
18	$[-\ln(1-\alpha)]^2$	−4.8026	0.9836	−3.3331	0.9699
19	$[-\ln(1-\alpha)]^3$	−7.2039	0.9836	−4.9996	0.9699
20	$[-\ln(1-\alpha)]^4$	−9.6053	0.9836	−6.6661	0.9699
21	$\ln[\alpha/(1-\alpha)]$	–	–	–	–
22	$\alpha^{1/4}$	−1.5484	0.9339	−0.9056	0.5324
23	$\alpha^{1/3}$	−1.5484	0.9339	−0.9056	0.6583
24	$\alpha^{1/2}$	−1.5484	0.9339	−0.9056	0.9984
25	$1-(1-\alpha)^{1/1}=\alpha$	–	–	–	–
26	$\alpha^{3/2}$	−4.6452	0.9339	−2.7167	0.8884
27	α^2	−3.0968	0.9339	−1.8111	0.8884
28	$1-(1-\alpha)^{1/4}$	−0.1773	1	−0.137	0.9705
29	$1-(1-\alpha)^{1/3}$	−0.2479	0.9997	−0.1897	0.9669
30	$3[1-(1-\alpha)^{1/3}]$	−0.2479	0.9997	−0.1897	0.9669
31	$1-(1-\alpha)^{1/2}$	−0.4148	0.9984	−0.3096	0.9576
32	$2[1-(1-\alpha)^{1/2}]$	−0.4148	0.9984	−0.3096	0.9576
33	$1-(1-\alpha)^2$	−1.1053	0.8649	−0.5383	0.7757
34	$1-(1-\alpha)^3$	−0.8504	0.7976	−0.3491	0.6769
35	$1-(1-\alpha)^4$	−0.6831	0.738	−0.239	0.6033
36	$(1-\alpha)^{-1}$	−2.2862	0.9812	−2.08	0.9951
37	$(1-\alpha)^{-1}-1$	−3.8346	0.9994	−2.9855	0.9966
38	$(1-\alpha)^{-1/2}$	−2.2862	0.9812	−2.08	0.9951
39	$\ln\alpha$	–	–	–	–
40	$\ln\alpha^2$	–	–	–	–
41	$(1-\alpha)^{-2}$	−4.5724	0.9812	−4.16	0.9951

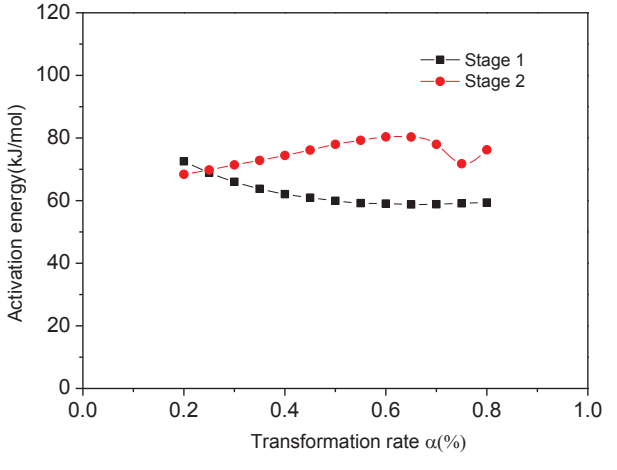

Figure 4: Line chart for thermal decomposition of NPL-10.

4 Conclusions

(a) The optimal conditions (in terms of both foam height and half-life) for the use of foaming agent NPL-10 in heavy oil recovery by steam injection are the following: T=220°C, pH 7, 10000 mg·L^{-1} salinity, and 10 g·L^{-1} oil content;

(b) NPL-10 starts decomposing above 220°C;

(c) Decomposition of NPL-10 occurs in two steps that follow a different kinetic law, with the rate of the first step being more sensitive to temperature than the rate of the second step.

The derived kinetic model provides a guidance for the selection of the optimal quantity of NPL-10 in heavy oil recovery by steam injection.

Acknowledgment: this work was supported by the Natural Science Foundation of Heilongjiang Province of China (Project No. E2015036), the National Science and Technology Major Projects of China for Oil and Gas (Projects No. 2016ZX05055-006 and 2016ZX05012-001), and the Cultivation Fund of Northeast Petroleum University of China.

Conflict of interest: Authors state no conflict of interest.

References

[1] Koottungal L., Special Report 2010 worldwide EOR survey. Oil & Gas Journal, 2010, 108(14), 41-53.

[2] Kamari A., Nikookar M., Sahranavard L., et al., Efficient screening of enhanced oil recovery methods and predictive economic analysis. Neural Computing and Applications, 2014, 25(3-4), 815-824.

[3] Hiraski G.J., The steam-foam process. Journal of Petroleum Technology, 1989, 41(05), 449-456.

[4] Ma K., Lopez-Salinas J. L., Puerto M. C., et al., Estimation of parameters for the simulation of foam flow through porous media. Part 1: the dry-out effect. Energy & Fuels, 2013, 27(5), 2363-2375.

[5] Farajzadeh R., Krastev R., Zitha P.L.J., Foam films stabilized with alpha olefin sulfonate (AOS). Colloids and Surfaces A: Physicochemical and Engineering Aspects, 2008, 324(1), 35-40.

[6] Farajzadeh R., Andrianov A., Krastev R., et al., Foam–oil interaction in porous media: Implications for foam assisted enhanced oil recovery. Advances in colloid and interface science, 2012, 183, 1-13.

[7] Ma K., Lopez-Salinas J.L., Puerto M.C., et al., Estimation of parameters for the simulation of foam flow through porous media. Part 1: the dry-out effect. Energy & Fuels, 2013, 27(5), 2363-2375.

[8] Worthen A.J., Bryant S.L., Huh C., et al., Carbon dioxide-in-water foams stabilized with nanoparticles and surfactant acting in synergy. AIChE Journal, 2013, 59(9), 3490-3501.

[9] El-Amin M.F., Salama A., Sun S., Numerical and dimensional analysis of nanoparticles transport with two-phase flow in porous media. Journal of Petroleum Science and Engineering, 2015, 128, 53-64.

[10] Keijzer P.P.M., Muijs H.M., Janssen-van Rosmalen R., et al.,Application of Steam Foam in the Tia Juana Field, Venezuela:Laboratory Tests and Field Results. SPE Enhanced Oil Recovery Symposium, 20-23 April, Tulsa, Oklahoma, 1986,SPE-14905.

[11] Maini B.B., Ma V., Thermal Stability of Surfactants for Steamflood Applications. SPE Oilfield and Geothermal Chemistry Symposium, 9-11 March, Phoenix, Arizona,1985, SPE-13572.

[12] Kleijnen J.P.C., Sensitivity analysis and related analyses: a review of some statistical techniques. Journal of Statistical Computation and Simulation, 1997, 57(1-4), 111-142.

[13] Tang B., Orthogonal array-based Latin hypercubes. Journal of the American statistical association, 1993, 88(424), 1392-1397.

[14] Kleijnen J.P.C., An overview of the design and analysis of simulation experiments for sensitivity analysis. European Journal of Operational Research, 2005, 164(2), 287-300.

[15] Einaga H., Futamura S., Ibusuki T., Heterogeneous photocatalytic oxidation of benzene, toluene, cyclohexene and cyclohexane in humidified air: comparison of decomposition behavior on photoirradiated TiO_2 catalyst. Applied Catalysis B: Environmental, 2002, 38(3), 215-225.

[16] Patel P., Hull T.R., McCabe R.W., et al., Mechanism of thermal decomposition of poly(ether ether ketone)(PEEK) from a review of decomposition studies. Polymer Decomposition and Stability, 2010, 95(5), 709-718.

[17] Zhao Z., Chaos M., Kazakov A., et al., Thermal decomposition reaction and a comprehensive kinetic model of dimethyl ether. International Journal of Chemical Kinetics, 2008, 40(1), 1-18.

[18] Robledo-Ortiz J.R., Zepeda C., Gomez C., et al., Non-isothermal decomposition kinetics of azodicarbonamide in high density polyethylene using a capillary rheometer. Polymer Testing, 2008, 27(6), 730-735.

[19] Kandelbauer A., Wuzella G., Mahendran A., et al., Model-free kinetic analysis of melamine–formaldehyde resin cure. Chemical Engineering Journal, 2009, 152(2), 556-565.

[20] Ptáček P., Bartoníčková E., Švec J., et al., The kinetics and mechanism of thermal decomposition of $SrCO_3$ polymorphs. Ceramics International, 2015, 41(1), 115-126.